Quaternary Research 79 (2013) 439–451

Contents lists available at SciVerse ScienceDirect

Quaternary Research

journal homepage: www.elsevier.com/locate/yqres

# Cosmogenic nuclide constraints on late Quaternary glacial chronology on the Dalijia Shan, northeastern Tibetan Plateau

Jie Wang [a,*], Christine Kassab [b], Jonathan M. Harbor [b], Marc W. Caffee [c], Hang Cui [a], Guoliang Zhang [a]

[a] Key Laboratory of Western China's Environmental Systems (Ministry of Education), Lanzhou University, Lanzhou, Gansu 730000, China
[b] Department of Earth, Atmospheric, and Planetary Sciences, Purdue University, West Lafayette, IN 47907, USA
[c] Department of Physics, Purdue Rare Isotope Measurement Laboratory, Purdue University, West Lafayette, IN 47907 1397, USA

ARTICLE INFO

*Article history:*
Received 13 September 2012
Available online 12 February 2013

*Keywords:*
Tibetan plateau
Cosmogenic nuclide
Glacial chronology
Dalijia Shan

ABSTRACT

Cosmogenic nuclide (CN) apparent exposure dating has become a widely used method for determining the age of glacial landforms on the Tibetan Plateau with >1200 published ages. We present the first $^{10}$Be exposure ages from the Dalijia Shan, the most northeastern formerly glaciated mountain range on the Tibetan Plateau. The moraine groups identified from field and remote sensing imagery mapping record four glacial events at 37.07 ± 3.70 to 52.96 ± 4.70 ka (MIS 3), 20.17 ± 1.79 to 26.99 ± 2.47 ka (MIS 2), 16.92 ± 1.49 to 18.76 ± 1.88 ka (MIS 2), and 11.56 ± 1.03 to 11.89 ± 1.06 ka (Younger Dryas). These ages indicate that glaciation in the northeastern Tibetan Plateau is much younger than previously thought. In addition, this record is consistent with many other regions on the Tibetan Plateau, with a local last glacial maximum during MIS 3 asynchronous with Northern Hemisphere last glacial maximum during MIS 2. The Dalijia Shan might also include an event of Younger Dryas age, but this needs to be tested in future studies.



## Introduction

Mountain glaciers are sensitive indicators of climate change, so understanding past variations in glacial extent is important for reconstructing past climates and predicting future climate change (Oerlemans, 2005). The glacial history of the Tibetan Plateau is important (1) regionally, in understanding and modeling how climate change impacts a region of over 2.5 million km$^2$ with an average elevation of ~4000 m asl, and (2) globally because of the impact that this large, high-elevation region has on climate worldwide. Outside of the polar regions the largest concentration of glaciers today is located on the Tibetan Plateau (46,640 km$^2$ glaciated; Shi et al., 2000), making it critical to understanding how glaciers will react to changing climate and whether this may produce a feedback that changes regional climate patterns. Currently the precipitation of the Tibetan Plateau and the glacial extent is controlled in part by competing atmospheric systems: mid-latitude westerlies, the South and East Asian monsoon, and Mongolia–Siberia high pressure system with perturbations from the El Nino–Southern Oscillation (Lehmkuhl and Owen, 2005; Owen and Benn, 2005; Kirchner et al., 2011). These same climate drivers influenced the paleoclimate of the Tibetan Plateau via shifts in their relative locations driving spatial and temporal patterns of glacial advance and retreat (Lehmkuhl and Owen, 2005; Zhang et al., 2006; Owen et al., 2008). Thus, if past glaciations have been controlled mainly by precipitation, reconstructing the extent and timing of past glaciations is important in constraining past changes in the dominance and patterns of these climate drivers.

Over the past century there has been much debate over the paleoextent of glaciers on the Tibetan Plateau, with reconstructions ranging from a plateau-wide ice sheet synchronous with Northern Hemisphere glaciation (e.g., Han, 1989; Kuhle, 1998, 2004) to limited glacier and ice cap expansions that are not synchronous in timing and extent with Northern Hemisphere glaciation (e.g., Rost, 2000; Owen et al., 2002a, 2005; Zheng et al., 2002; Finkel et al., 2003; Zech et al., 2003; Zhang et al., 2005; Owen, 2009; Heyman et al., 2011a). Based upon a large body of research, including recent detailed studies focused on mapping glacial landforms in the field and with remote sensing, as well as absolute dating of landforms using a variety of methods, it is widely accepted that a large ice sheet did not cover the Tibetan Plateau during the past few glacial cycles. Rather, the glacial record of the Tibetan Plateau is dominated by the expansion and contraction of glaciers and small ice caps (e.g., Derbyshire et al., 1991; Shi et al., 1992; Lehmkuhl, 1998; Lehmkuhl et al., 1998; Zheng and Rutter, 1998; Schäfer et al., 2002; Zhou et al., 2004; Lehmkuhl and Owen, 2005; Owen et al., 2005, 2008, 2012).

Various methods have been used to date glacial deposits and landforms on the Tibetan Plateau, including relative age control from stratigraphy or morphostratigraphy, organic radiocarbon ($^{14}$C), thermoluminescence (TL), optically stimulated luminescence (OSL), electron spin resonance (ESR), and cosmogenic nuclide (CN). The earliest work relied on the general global model of

* Corresponding author.
*E-mail addresses:* wangjie@lzu.edu.cn (J. Wang), ckassab@purdue.edu (C. Kassab).

0033-5894/$ – see front matter 
http://dx.doi.org/10.1016/j.yqres.2013.01.004

glaciation chronology to assign relative ages to various landforms and deposits. Low abundance of organic matter within glacial deposits provided a few absolute radiocarbon ages for young events, but care had to be taken when interpreting the results because of the possibility of a considerable time lapse between the demise of the organism being dated and the glacial event it is associated with (Richards, 2000). The sparseness of suitable sediments and the inability to correlate some glaciofluvial sediments with specific glacial events limit the applicability of TL and OSL methods. Where successful, these methods have provided ages that represent the timing of deposition of sediment associated with a glacial event (Richards, 2000; Owen and Benn, 2005). Currently the most widely used technique to date glacial advances is CN exposure dating. Unlike TL and OSL methods that provide the timing of deposition, exposure dating methods provide a minimum age of deglaciation (Owen and Benn, 2005). All three of these methods extend the chronological control to identify older glaciations and allow for the dating of rocks and sediments that do not have organic matter or are beyond the traditional $^{14}C$ range.

Over the past two decades, multiple studies have used exposure dating methods to constrain the timing of glaciation across the Tibetan Plateau and have produced more than 1200 published exposure ages (discussed in Chevalier et al., 2011; Heyman et al., 2011b). Several glacial advances in various regions across the Tibetan Plateau can be identified based upon the exposure ages: the Little Ice Age, Neoglacial, mid-Holocene, early Holocene, late glacial interstadial, global last glacial maximum (LGM; MIS 2), mid-last glacial (MIS 3), and early last glacial (MIS 4). Based mainly on the absence of dated landforms in some areas, not all of these glaciations appear to have occurred in every region (Owen et al., 2005) or they have very different relative magnitudes in different areas. Spatial variations in timing and magnitude of glaciation can be linked to the different climate systems that impact the Tibetan Plateau. Regions that are primarily affected by the monsoonal systems recorded glacial advances during interstadial periods as a result of increased precipitation due to increased insolation during these periods. Precipitation in these regions decreased during glacial periods, resulting in a smaller glacier advance if any (Shi et al., 2001; Owen et al., 2002a,b; Shi, 2002). Regions that are primarily affected by the winter westerlies typically experience glacier advances during glacial periods because precipitation is not influenced by changes in insolation (Owen et al., 2005, 2012; Seong et al., 2009).

The Dalijia Shan (Shan = mountain), along the northeast boundary of the Tibetan Plateau, is not presently glaciated. However, during the glacial–interglacial cycles of the Quaternary, it was extensively and repeatedly glaciated. Glacial landforms from multiple glaciations are well preserved, especially in the Dalijia Pass area (e.g., Deheisui Valley). The Quaternary glacial landforms and moraines of the Dalijia Shan have been studied since the late 1980s and have been assigned to three glacial stages with local names: Wulongguan (oldest), Pass, and Dalijia (youngest; Li and Pan, 1989; Shen et al., 1989; Pan, 1993). To date, there is little absolute age control on the glacial landforms; researchers have only used relative age dating techniques to interpret a glacial history for this region. These studies are based on correlation of loess deposited on top of the moraines with loess deposits within terraces along the Daxia River and weathering profiles of soils that have developed on top of the moraines (Li and Pan, 1989; Shen et al., 1989; Mahaney and Rutter, 1992; Pan, 1993).

$^{10}Be$ exposure ages of 22 samples collected on four moraine groups in the Dalijia Shan presented here provide the first absolute age control for Dalijia Shan glacial landforms that can be compared with ages from other regions on the Tibetan Plateau. These ages from the northeastern-most region of the Tibetan Plateau that is known to have been glaciated add to the growing database of numerical ages from across the Tibetan Plateau, contributing to a better understanding of the chronological framework.

## Geologic setting

The Dalijia Shan is located in a transition region between the northeastern border of the Tibetan Plateau and the Loess Plateau (Fig. 1A; Li and Pan, 1989; Pan, 1993). Average elevation is approximately 3600 m asl with Dalijia Peak reaching 4636 m asl. There is a planation surface between 4000 and 4300 m asl on top of the Dalijia Shan, which slopes ~4° from north to south (Fig. 1B). Bedrock in this region consists mainly of intensely folded and faulted Precambrian crystalline complexes of granite and schist. Deformation is mainly a result of late Neogene orogenic events (Mahaney and Rutter, 1992).

The climate of this region is semi-arid, and dominated by the East Asia and South Asia monsoons. Moisture is derived mainly from the South Asia monsoon (Indian Ocean and Bengal Bay; Wang et al., 2005; Zhang et al., 2011). At Linxia Station (35°34′N, 103°11′E; 1917 m asl) on the eastern slope of Dalijia Shan (~40 km east of Dalijia Peak), the mean annual temperature is 7.1°C, and the mean annual precipitation is 499 mm (for the period 1951–2011) (http://cdc.cma.gov.cn). Precipitation between May and October accounts for >85% of the annual total; winter and spring are very dry. Many types of glacial landforms and deposits (planation surfaces, U-shaped valleys, moraines, tills, and rouche mountonnées) have been identified above 3000 m asl in the Dalijia Shan, with the majority located around Dalijia Peak (elev. ~4600 m asl; Li and Pan, 1989; Pan, 1993). Based on the presence of glacial landforms and deposits, Li and Pan (1989) and Pan (1993) hypothesized that a 150 $km^2$ ice cap covered the planation surface.

Moraines characterized by deeply weathered tills were identified by Li and Pan (1989) at Wulongguan (~2700 m asl) and provide the basis for the Wulongguan glacial stage. Our own field investigations at Wulongguan did not identify any unequivocal glacial deposits or landforms and so the Wulongguan glacial stage is not included in our analysis.

In the Dalijia Pass region, the oldest moraine set, group A, is a lateral moraine that is only preserved at altitudes of 3600–3900 m asl (Figs. 1C and 2). It is ~400–600 m above the valley floor, and cannot be continuously traced to an end moraine, possibly due to post-depositional glacial and fluvial erosion of the landform. The tills at this site are gray and sub-angular, with clasts of granite and overlie schistose bedrock. Many weathered, erratic granite boulders, 2–4 m in diameter, and a thick loess layer are present on the platform surface. The glacial advance associated with this deposit was referred to as the Pass glacial stage by Li and Pan (1989) and Pan (1993).

Another lateral moraine, moraine group B, is present on the eastern and western sides of the Deheisui valley. These moraines are adjacent to and slightly lower than the group A moraines and represent a younger, less extensive glacier configuration. Moraine group C includes well-developed right and left lateral moraines that join end moraines at altitudes of 3180–3400 m asl in the Qitai valley. These end moraines consist of three distinct moraine ridges, ~20–40 m above the valley floor with ~0.5-m thick meadow soils. The sediments of these ridges are poorly sorted, with granite clasts ranging in size from fine-grained sands to boulders of ~1 m in diameter. Boulders present on the surface of this moraine exhibit slight granular weathering. The two moraine sets, groups B and C, were assigned to the early and late Dalijia glacial stage by Li and Pan (1989) and Pan (1993).

Near the head of the valley is the group D moraine, a latero-frontal moraine ridge that rises ~20–40 m above the valley floor at an altitude of 3800 m asl. The till includes granite clasts and areas of fine sand, and a soil profiles that is several cm thick.

Glacial deposits in the actual pass area (Dalijia Pass moraine) have been previously assigned to the Pass glacial stage and have been linked to moraine group A deposits in past studies. However the elevation of these moraines is more consistent with moraine group B deposits. One of the goals of this study is to determine whether these deposits are equivalent in age to moraine group A or B.

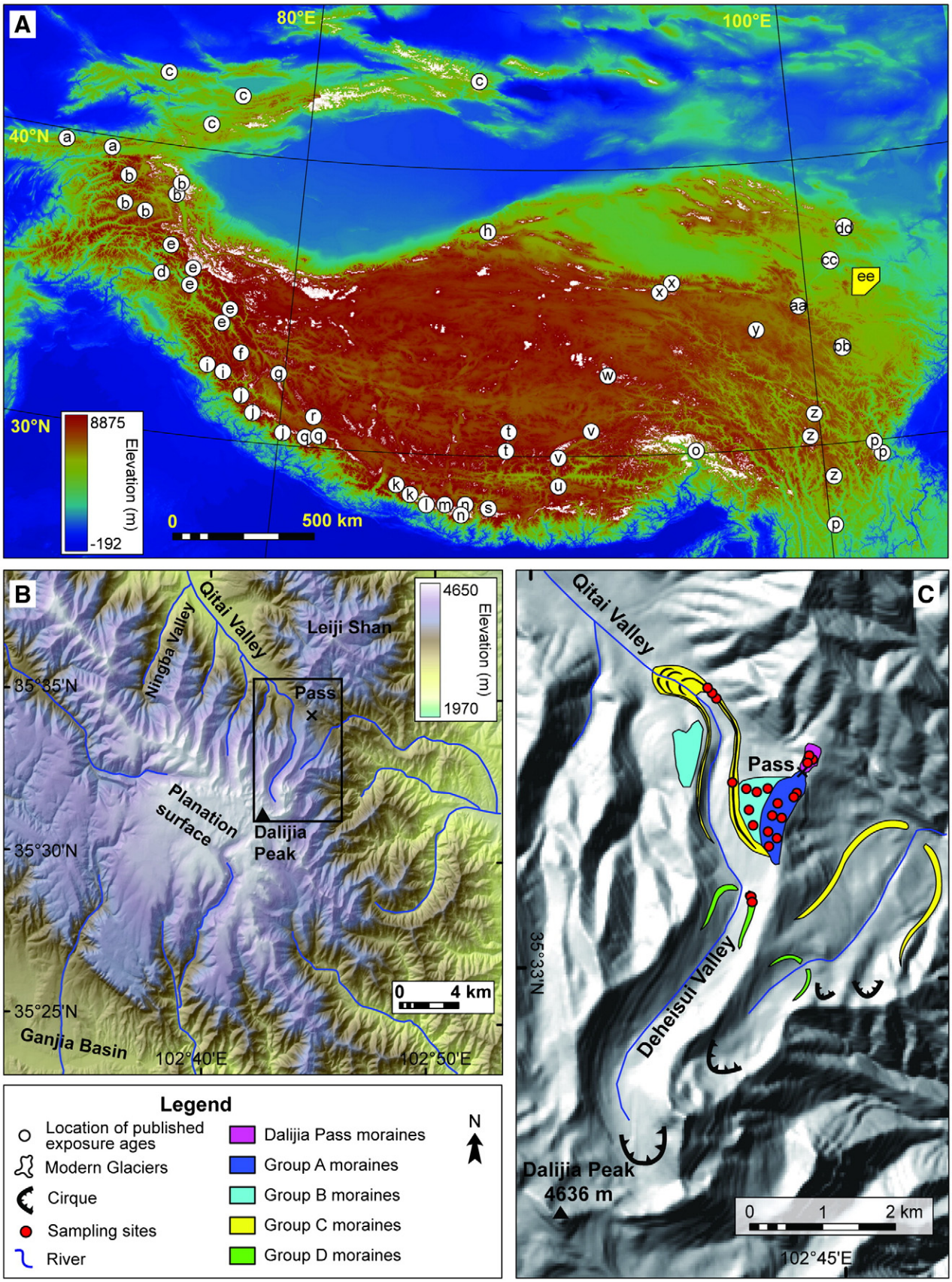


**Figure 1.** A) DEM of the Tibetan Plateau showing the location of the Dalijia Shan (yellow polygon) along the northeastern margin and the location of published cosmogenic nuclide exposure-age studies (white dots). The letters correspond to the mountain ranges in Figs. 6 and 7. B) DEM of the Dalijia Shan region. Note that the majority of the glacial landforms are located around Dalijia Peak. C) DEM illustrating the location of the different moraine groups sampled from for this study and the locations of the samples collected (red dots). Location is indicated in (B) by the black box.

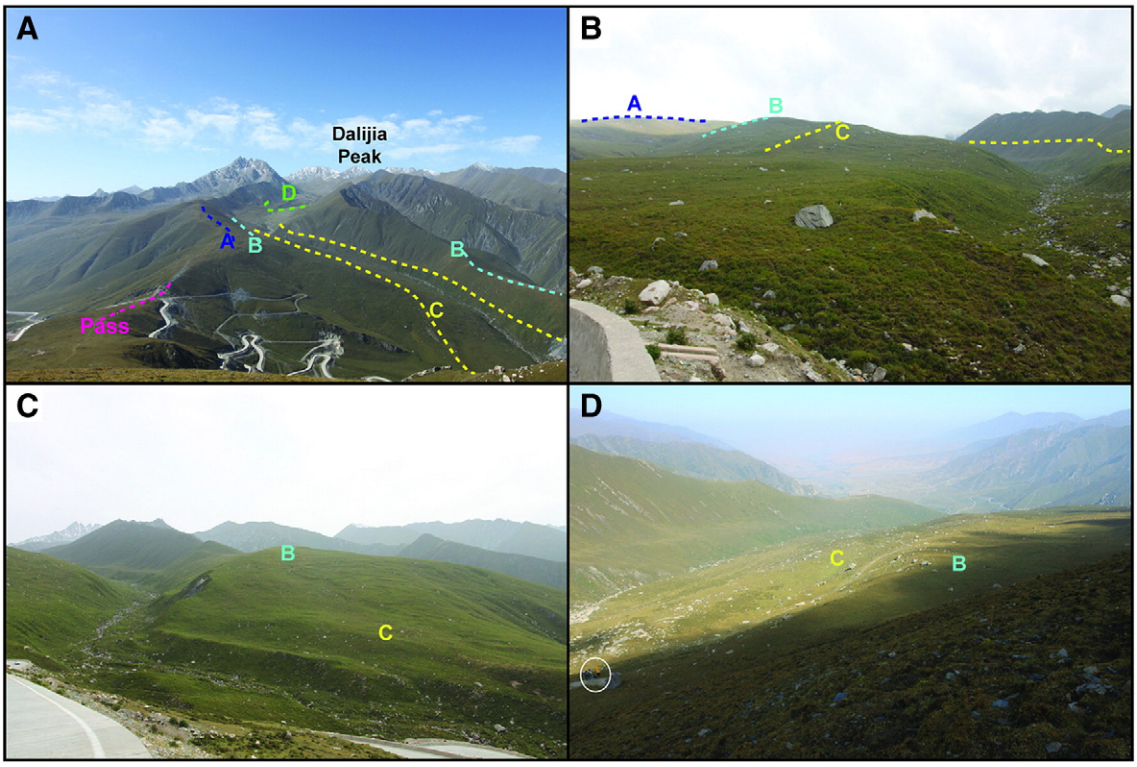


**Figure 2.** Photographs illustrating the landforms present in the Deheisui Valley. The colored dashed lines identify the different moraine groups that are illustrated in Fig. 1 following the same color scheme. A) Overview of the Deheisui valley looking to the south. All of the moraine groups are present in this photograph. This is one of the few valleys in the mountain range with well-preserved glacial landforms. B) View of the valley looking to the southeast. Moraine groups A, B, and C can be seen in this photo. C) View of the valley looking to the south of moraine groups B and C. D) View of the valley looking to the northwest at moraine groups B and C. People (white circle) for scale.

Numerical age control on glacial deposits in the Deheisui Valley has been lacking; most previous studies have focused on relative age control because these were the only methods available at the time the work was done. Mahaney and Rutter (1992) added to this work by examining soil morphology, weathering, and geochemistry of the moraines and glacial deposits in Dalijia Pass and concluded that the lack of differences in soil morphology, weathering of the B horizon and amino acid D/L ratios imply that the soils are all of the same age and therefore related to the same glacial event (Mahaney and Rutter, 1992). In other studies, the landforms of the Dalijia Pass have been correlated with multiple terraces of various ages along the Daxia River (to the south). Loess and organic matter from within the terraces has been dated using thermoluminescence and $^{14}C$ dating techniques. Six terraces have been identified along the Daxia River, of which the lower three are correlated to the glacial landforms and deposits in the Dalijia Shan based upon altitude, degree of weathering, morphology, and loess thickness overlying the landforms. The hypothesized ages of glaciations are 140 ka (Pass glacial stage), 83–56 ka and 30–13 ka (Dalijia glacial stage), and have been correlated with the Riss and Würm glacial stages of the European Alps (Li and Pan, 1989; Shen et al., 1989; Pan, 1993).

## Methods

Geomorphic investigations in the field area, combined with mapping from digital elevation models (DEMs) and remote sensing images, provide a basis for understanding the morphostratigraphic relationships between glacial landforms. The glacial geomorphology mapped by Li and Pan (1989) and Pan (1993) in the Dalijia Shan was examined and remapped in the field, aided by a DEM (constructed from the 10-m interval contours and spot heights of four 1:50,000 topographical maps), a 1:200,000 map of the Chinese Geological Survey as well as Google Earth™ imagery.

The geomorphic map aided in the selection of the sample collection sites in the Dalijia Shan for $^{10}Be$ exposure dating. All of the samples were collected from moraines within the Deheisui Valley on the west side of Dalijia Pass to determine the timing of glaciations in this mountain range and to compare spatial patterns and similarities with other chronologies regionally and across the Tibetan Plateau. Samples were collected solely from the Deheisui Valley because it is the only valley that has evidence of multiple glaciations. Four lateral moraines are present within the valley and multiple samples (2–5) were collected from each. A total of 22 samples were collected from the top surfaces of large granitic boulders close to the crest of the moraine ridge. Care was taken to choose large intact boulders that were unlikely to have been transported downslope or exhumed subsequent to deposition of the moraine (Figs. 3 and 4). The location and elevation of each boulder were recorded using a hand-held GPS unit. Shielding by the surrounding topography was measured with a hand-held inclinometer on compass bearings at 10° intervals.

Processing of the rock samples to isolate $^{10}Be$ was carried out at the Purdue Rare Isotope Measurement Laboratory (PRIME Lab). First, the samples were crushed and sieved. Quartz was then separated from 250–500 μm size fractions using the methods of Kohl and Nishiizumi (1992), and this was followed by Be carrier addition, ion exchange chromatography, and conversion to BeO. Niobium (Nb) powder was mixed with the BeO and the combination was pounded into stainless steel targets for measurement of $^{10}Be/^{9}Be$ ratios by accelerator mass spectrometry at PRIME Lab based on revised ICN standards (Nishiizumi et al., 2007). All $^{10}Be$ exposure ages were calculated by applying the Lal (1991) and Stone (2000) time-dependent model using the CRONUS-Earth web-based calculator (Balco et al., 2008), version 2.2 (constants file version 2.2.1) with a $^{10}Be$ half-life of 1.387 Ma (Chmeleff et al., 2010; Korschinek et al., 2010), taking account of the $^{10}Be$ standardization, and assuming an absence of inheritance and post-depositional surface erosion, and using a rock density of 2.65 g/cm$^3$ (average value of 3 samples measured).

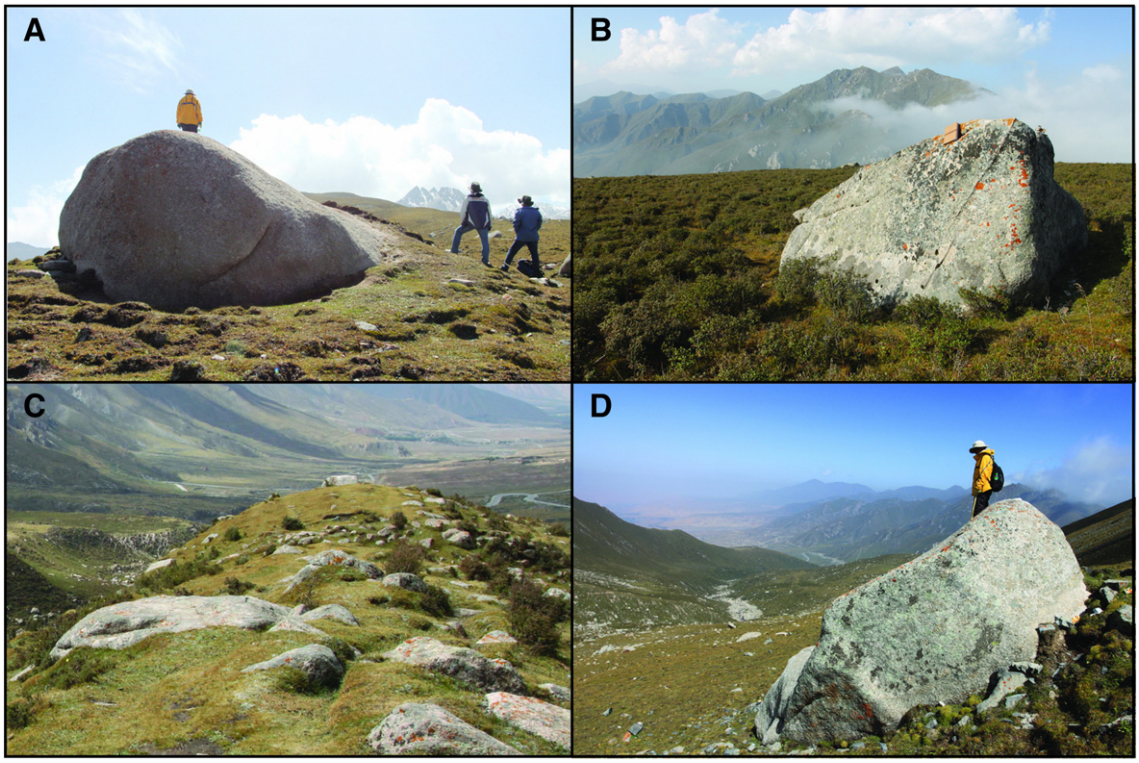


**Figure 3.** Representative photographs of some of the boulders sampled in the Deheisui Valley. A) Moraine group A, the oldest. B) Moraine group B. C) Moraine group C. D) Moraine group D, the youngest.

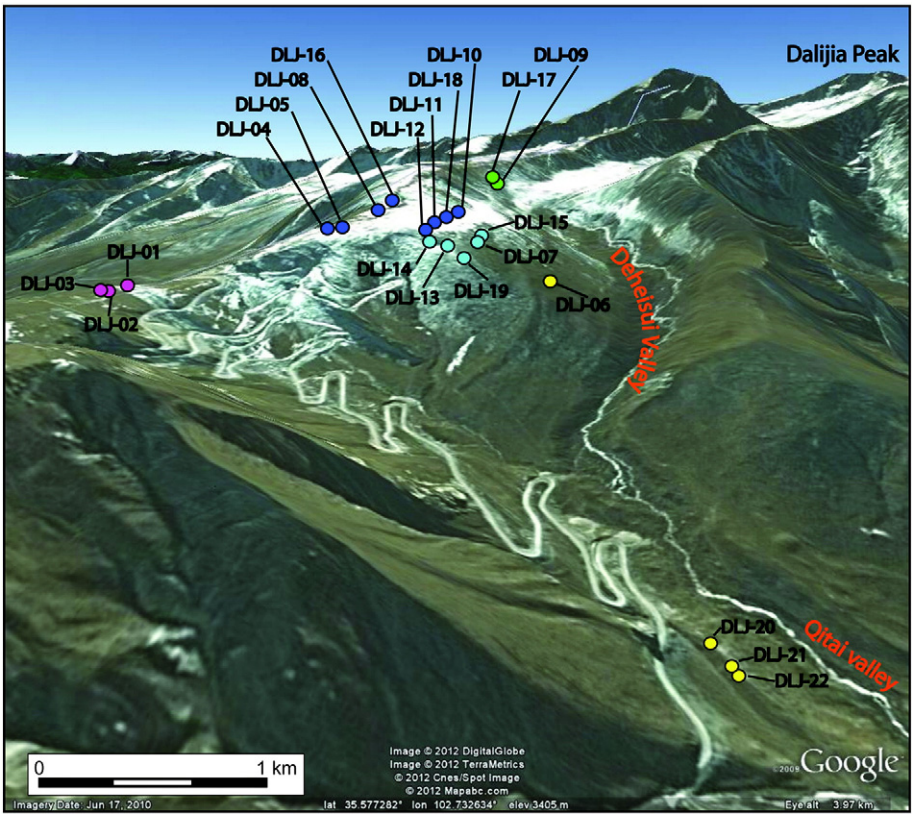


**Figure 4.** 3D oblique view of the Deheisui valley looking to the south with sample locations. Samples are colored according to the moraine group identified in Fig. 1: moraine group A, dark blue; B: light blue; C: yellow; D: green; Pass: purple. Note that the only preserved landforms from older glacial events are the lateral moraines located high up on the valley wall.

Air-pressure changes with elevation are calculated following the standard atmosphere equation, with sea-level air pressure and temperature derived from the NCAR/NCEP reanalysis data product (http://www.cdc.noaa.gov/ncep_reanalysis/). The approximate age of each moraine is determined by plotting the data for each group on a Gaussian probability plot, using the peak of the sum of all of the values as the age.

## Results

The results are given in Table 1 (sample parameters and measured $^{10}$Be concentrations), Table 2 ($^{10}$Be exposure ages), and Figure 5 (probability plots for the different moraine groups). Because there are several distinct production rate scaling schemes in the literature, there are a number of possibilities for assigning apparent exposure ages to the measured $^{10}$Be concentrations. We present results produced using the major production rate scaling schemes (Table 2); differences range from up to 20% for ages older than 40 ka, ~10% for ages around 20 ka, and ~6% for the youngest ages, ~10 ka. We use the Lal (1991) and Stone (2000) time-dependent model (last columns in Table 2) in the discussion of our data in order to allow for easy comparison to previously published exposure age data sets. However, as Table 2 illustrates, the number of events and their general age assignments to major glacial stages are the same regardless of the production rate scheme that is used.

The distribution of exposure ages from the four moraine groups is consistent with their stratigraphic sequence. Out of 22 samples, 21 produced consistent results that did not appear to be influenced by incomplete exposure or inheritance. DLJ-04 is significantly older than the cluster of ages obtained from the same moraine, and from any other samples collected. Although it is possible that this one rock is the only sample providing evidence of a much older event, it is more likely that it is an outlier that has an erroneous age due to cosmogenic inheritance (the rock was exposed at the surface for a considerable period before it was moved by the glacier and incorporated into the moraine). For this reason DLJ-04 is not included in any of the subsequent discussion and analysis. The ages of the remaining samples indicate that there are four glacial events over the past 100 ka recorded in the study area, with little disparity within each age cluster.

Moraine group A is the oldest lateral moraine within the valley. Ages range from 37.07 ± 3.70 to 52.96 ± 4.70 ka (two moraines near the crest of the valley wall, ~3750 m asl). Based on the probability plot, the associated glacial event occurred at ~38.6 +32.4/−6.85 ka (Fig. 5A).

In previous work, the hypothesized age of the Dalijia Pass moraine group (in Dalijia Pass, ~3610 m asl) placed it with moraine group A (Li and Pan, 1989; Pan, 1993). However, based on the age range of the $^{10}$Be exposure samples, from 22.38 ± 2.01 to 26.99 ± 2.47 ka, it is most likely associated with moraine group B. The peak age of the probability plot indicates that the associated glacial event occurred at ~23.5 +3.38/−1.43 ka (Fig. 5A). Moraine group B is a lateral moraine and is the next youngest moraine within the valley. It is located part way down the valley side (~3660 m asl), ~5 km from the present day cirque. Ages within this group range from 20.17 ± 1.79 to 26.18 ± 2.47 ka. Based upon the probability plot the associated glacial event occurred at ~21.8 +3.24/−1.42 ka (Fig. 5B).

Moraine group C contains boulders that are at the lowest elevation, a single boulder (DLJ-06) from the lateral moraine at ~3580 m asl and samples from the terminal moraine which is the only one preserved down valley, ~7 km from the present day cirque (~3305 m asl). Ages for the terminal moraine range from 16.92 ± 1.49 to 17.24 ± 1.53 ka. The cluster of ages for this moraine is tight and indicates that deglaciation from this moraine began at ~17 ka. Sample DLJ-06, located ~5.3 km from the present day cirque, on the lateral moraine has an age of 18.76 ± 1.88 ka. Based on the probability plot, the associated glacial event occurred at ~17.3 +1.05/−0.61 ka (Fig. 5C).

Moraine group D is an end moraine of the youngest glacial event located ~4 km from the cirque. Two samples from this moraine yielded ages of 11.56 ± 1.03 ka and 11.89 ± 1.06 ka. These ages are tightly clustered representing a glacial event, possibly an advance or stillstand during retreat, that occurred at ~11.7 +0.24/−0.22 ka (Fig. 5D).

## Discussion

### *Inheritance and incomplete exposure*

Two factors that have to be considered when analyzing apparent age results are inheritance and incomplete exposure. A boulder with remnant cosmogenic nuclide concentration as a result of prior exposure not completely reset by erosion of the outer surface of the rock will yield apparent exposure ages that exceed the depositional age. These ages represent the maximum limiting deglaciation age (Fabel and Harbor, 1999; Heyman et al., 2011a,b). Heyman et al. (2011b)

**Table 1**
$^{10}$Be concentrations, coordinates and other parameters for all sample boulders from the Dalijia Shan.

| Sample no. | Moraine group | Latitude (°N) | Longitude (°E) | Elevation (m asl) | Boulder size l/w/h (m) | Sample thickness (cm) | Shielding correction | $^{10}$Be concentration[a] ($10^5$ atoms g$^{-1}$) |
|---|---|---|---|---|---|---|---|---|
| DLJ-01 | Pass | 35.5745 | 102.7437 | 3617 | 3.0/2.0/1.0 | 1.9 | 0.99975 | 10.925 ± 0.324 |
| DLJ-02 | Pass | 35.5751 | 102.7439 | 3614 | 4.0/2.9/1.6 | 2.0 | 0.99905 | 11.683 ± 0.335 |
| DLJ-03 | Pass | 35.5746 | 102.7446 | 3608 | 3.0/2.9/1.7 | 1.6 | 0.99926 | 13.346 ± 0.452 |
| DLJ-04 | A | 35.5692 | 102.7395 | 3719 | 6.0/5.0/3.5 | 1.7 | 1.00000 | 46.736 ± 2.038 |
| DLJ-05 | A | 35.5690 | 102.7390 | 3720 | 7.0/5.1/2.5 | 2.4 | 0.99970 | 20.075 ± 1.036 |
| DLJ-06 | C | 35.5700 | 102.7311 | 3580 | 4.0/3.1/2.0 | 1.8 | 0.99889 | 8.877 ± 0.472 |
| DLJ-07 | B | 35.5683 | 102.7340 | 3669 | 5.0/3.0/2.5 | 1.3 | 0.99947 | 13.377 ± 0.553 |
| DLJ-08 | A | 35.5671 | 102.7383 | 3759 | 7.0/3.0/1.6 | 3.2 | 0.99070 | 22.503 ± 0.547 |
| DLJ-09 | D | 35.5577 | 102.7354 | 3828 | 3.0/2.7/1.6 | 2.1 | 0.99070 | 6.058 ± 0.172 |
| DLJ-10 | A | 35.5648 | 102.7356 | 3735 | 3.0/1.7/1.1 | 2.6 | 0.99851 | 20.219 ± 0.549 |
| DLJ-11 | A | 35.5670 | 102.7360 | 3713 | 6.0/3.9/2.0 | 1.6 | 0.99806 | 29.240 ± 0.689 |
| DLJ-12 | A | 35.5683 | 102.7360 | 3701 | 3.1/2.5/1.7 | 2.2 | 0.99838 | 24.525 ± 0.607 |
| DLJ-13 | B | 35.5693 | 102.7349 | 3667 | 5.2/3.0/1.8 | 3.4 | 0.99877 | 9.909 ± 0.268 |
| DLJ-14 | B | 35.5691 | 102.7356 | 3680 | 3.3/2.7/1.5 | 1.9 | 0.99941 | 11.886 ± 0.298 |
| DLJ-15 | B | 35.5676 | 102.7340 | 3682 | 2.8/2.1/1.6 | 1.4 | 0.99905 | 11.490 ± 0.338 |
| DLJ-16 | A | 35.5656 | 102.7382 | 3783 | 4.9/3.0/1.6 | 2.5 | 0.99070 | 23.382 ± 0.600 |
| DLJ-17 | D | 35.5583 | 102.7351 | 3816 | 3.3/3.1/1.4 | 2.2 | 0.99070 | 6.181 ± 0.171 |
| DLJ-18 | A | 35.5660 | 102.7358 | 3734 | 3.5/2.2/1.1 | 2.3 | 0.99851 | 20.840 ± 0.604 |
| DLJ-19 | B | 35.5701 | 102.7341 | 3649 | 4.6/2.9/2.1 | 2.8 | 0.99877 | 10.341 ± 0.326 |
| DLJ-20 | C | 35.5829 | 102.7271 | 3304 | 1.9/1.8/0.8 | 2.0 | 0.99421 | 6.909 ± 0.181 |
| DLJ-21 | C | 35.5832 | 102.7268 | 3306 | 1.5/1.4/0.9 | 2.0 | 0.99421 | 6.930 ± 0.182 |
| DLJ-22 | C | 35.5833 | 102.7267 | 3305 | 2.1/1.7/1.0 | 2.5 | 0.99421 | 6.760 ± 0.164 |

[a] See Supplementary Table 1 for complete $^{10}$Be data including sample and carrier weight and sample and blank $^{10}$Be/$^{9}$Be values.

**Table 2**
$^{10}$Be surface exposure ages calculated with different scaling methods.

| Sample no. | Moraine group | Lal (1991) and Stone (2000) constant production rate | Desilets and Zreda (2003), Desilets et al. (2006) | Dunai (2001) | Lifton et al. (2005) | Lal (1991) and Stone (2000) time-varying production rate |
|---|---|---|---|---|---|---|
| | | Exposure age (ka) | Exposure age (ka) | Exposure age (ka) | Exposure age (ka) | Exposure age (ka) |
| DLJ-01 | Pass | 23.15 ± 2.14 | 21.42 ± 2.62 | 21.57 ± 2.63 | 20.73 ± 2.15 | 22.38 ± 2.01 |
| DLJ-02 | Pass | 24.84 ± 2.29 | 22.81 ± 2.78 | 22.90 ± 2.78 | 22.08 ± 2.28 | 23.86 ± 2.14 |
| DLJ-03 | Pass | 28.40 ± 2.67 | 25.71 ± 3.18 | 25.69 ± 3.16 | 24.83 ± 2.60 | 26.99 ± 2.47 |
| DLJ-04 | A | 95.28 ± 9.48 | 78.89 ± 10.12 | 76.95 ± 9.82 | 75.02 ± 8.24 | 85.49 ± 8.29 |
| DLJ-05 | A | 40.60 ± 4.14 | 34.96 ± 4.54 | 34.54 ± 4.47 | 33.65 ± 3.78 | 37.07 ± 3.70 |
| DLJ-06 | C | 19.18 ± 1.96 | 18.08 ± 2.35 | 18.36 ± 2.38 | 17.53 ± 1.97 | 18.76 ± 1.88 |
| DLJ-07 | B | 27.47 ± 2.66 | 24.85 ± 3.12 | 24.86 ± 3.11 | 24.00 ± 2.58 | 26.18 ± 2.47 |
| DLJ-08 | A | 45.32 ± 4.14 | 38.16 ± 4.64 | 37.68 ± 4.56 | 36.77 ± 3.77 | 40.65 ± 3.60 |
| DLJ-09 | D | 11.56 ± 1.06 | 11.14 ± 1.36 | 11.67 ± 1.41 | 10.85 ± 1.12 | 11.56 ± 1.03 |
| DLJ-10 | A | 40.68 ± 3.74 | 34.99 ± 4.27 | 34.57 ± 4.20 | 33.68 ± 3.47 | 37.14 ± 3.32 |
| DLJ-11 | A | 59.34 ± 5.42 | 48.67 ± 5.92 | 47.70 ± 5.78 | 46.23 ± 4.74 | 52.96 ± 4.70 |
| DLJ-12 | A | 50.21 ± 4.59 | 41.68 ± 5.08 | 41.13 ± 4.99 | 40.04 ± 4.11 | 44.50 ± 3.95 |
| DLJ-13 | B | 20.70 ± 1.89 | 19.28 ± 2.34 | 19.52 ± 2.36 | 18.67 ± 1.92 | 20.17 ± 1.79 |
| DLJ-14 | B | 24.36 ± 2.22 | 22.33 ± 2.71 | 22.44 ± 2.71 | 21.60 ± 2.21 | 23.44 ± 2.07 |
| DLJ-15 | B | 23.44 ± 2.20 | 21.56 ± 2.66 | 21.71 ± 2.67 | 20.87 ± 2.19 | 22.63 ± 2.07 |
| DLJ-16 | A | 46.25 ± 4.24 | 38.73 ± 4.72 | 38.24 ± 4.64 | 37.30 ± 3.83 | 41.34 ± 3.68 |
| DLJ-17 | D | 11.89 ± 1.09 | 11.45 ± 1.39 | 11.98 ± 1.45 | 11.14 ± 1.14 | 11.89 ± 1.06 |
| DLJ-18 | A | 41.86 ± 3.87 | 35.84 ± 4.39 | 35.40 ± 4.32 | 34.52 ± 3.58 | 38.02 ± 3.42 |
| DLJ-19 | B | 21.71 ± 2.02 | 20.16 ± 2.47 | 20.37 ± 2.49 | 19.52 ± 2.03 | 21.09 ± 1.91 |
| DLJ-20 | C | 17.49 ± 1.59 | 16.92 ± 2.05 | 17.22 ± 2.08 | 16.45 ± 1.68 | 17.21 ± 1.53 |
| DLJ-21 | C | 17.52 ± 1.60 | 16.94 ± 2.06 | 17.25 ± 2.08 | 16.47 ± 1.69 | 17.24 ± 1.53 |
| DLJ-22 | C | 17.17 ± 1.56 | 16.64 ± 2.01 | 16.95 ± 2.04 | 16.18 ± 1.65 | 16.92 ± 1.49 |

$^{10}$Be surface exposure ages were calculated by applying the CRONUS-Earth web-based calculator (Balco et al., 2008), version 2.2 (constants file version 2.2.1) using a $^{10}$Be half-life of 1.387 Ma (Chmeleff et al., 2010; Korschinek et al., 2010), taking account of the $^{10}$Be standardization, and assuming an absence of inheritance and post-depositional surface erosion, a density of 2.65 g/cm$^3$.

suggested that incomplete exposure was more important than prior exposure, and most authors conceived of nuclide inheritance as a process that produces rare and easily recognizable outliers with wildly different exposure ages than the bulk of boulders on a moraine, especially on alpine–glacial moraine sequences (e.g., Porter and Swanson, 2008). Out of the 22 samples only one, DLJ-04, appears to have significant inheritance. The other boulders from the same moraine yield a cluster of younger ages centered on ~39 ka, leading to the conclusion that the age of DLJ-04 (~85 ka) is due to inheritance from previous exposure. Incomplete exposure or erosion of the boulder surface can also impact the results, resulting in an apparent exposure age that underestimates the depositional age. These ages thus represent a minimum limiting deglaciation age (Fabel and Harbor, 1999; Heyman et al., 2011a, b). If the boulder sampled was buried more than 10 cm within the moraine when it was deposited and has since been brought to the surface through degradation of the moraine, the concentration of cosmogenic nuclides will be low. Strategies for detecting excess scatter have focused on statistical methods for determining whether the variance in a group of measurements is equal to that expected from the measurement uncertainty, the most commonly used of which is the reduced chi-squared statistic ($x_R^2$). If measurement uncertainty is the only source of scatter, the expected value of this statistic is ~1. Thus, exposure-age data sets with reduced chi-squared values close to 1 could be averaged to yield a more accurate age for the landform (Balco, 2011). The exposure age for groups Pass A (excluding the old sample DLJ-04), B, C and D have $x_R^2$ values of 1.09, 0.50, 1.21, 0.23 and 0.05. For each moraine there is relatively close clustering of ages; therefore, we believe that the boulders have not been impacted significantly from incomplete exposure and/or erosion.

The apparent exposure ages of boulders from the moraines in Deheisui Valley are significantly younger than those proposed by previous researchers using relative dating techniques which relied primarily on the correlation of moraines with terrace deposits along the Daxia River. Based upon the apparent exposure ages, glacial events in the Dalijia Shan occurred during MIS 3 (~38.6 ka), MIS 2 (~23.5–21.8 and ~17.3 ka) and late MIS 2/Holocene (~11.7 ka). These ages are a more accurate reflection of the timing of glacial advance in the Dalijia Shan than earlier relative age and correlation estimates. The glacial events dated in the terraces may record older events for which the associated landforms may no longer exist. In order for the moraines to be much older than the apparent exposure age and closer to the hypothesized ages (MIS 6 or MIS 4), all of the boulders must have experienced some form of incomplete exposure, either through post-depositional burial or erosion of the boulder surface. However, both the geomorphic context of the boulders and the statistics of the measured age distribution lead us to the conclusion that the observed scatter largely reflects measurement uncertainties and not geomorphogenic uncertainties.

### *Chronology of the Dalijia Shan*

At least four glacial events have been preserved in the Deheisui Valley. The oldest glacial event, at ~38.6 ka (MIS 3), was probably the most extensive. The lateral moraine (moraine group A) associated with this event is the highest one on the valley side which suggests that it filled the valley more than younger glacial events and therefore extended farther down valley. No glacial landforms associated with this event are preserved down valley of the MIS 2 terminal moraine; the terminal moraine may have been completely eroded or buried by fluvial deposits. The other explanation for the absence of MIS 3 terminal moraines is that younger advances may have extended farther down valley, destroying any glacial landforms in their path. Based upon the location of the ~38.6 ka moraines (moraine group A), it appears that the glacier may have spilled over the valley crest into the neighboring valley at its maximum extent. Boulders in the Dalijia Pass (Dalijia Pass moraine group) are not numerically linked with these older moraines even though earlier researchers had connected these deposits based on similar weathering characteristics. The ages of these boulders (23.5 ka) are similar to those in moraine group B (the next youngest glacial event at ~21.8 ka) and are also located at the slightly lower elevation (~3600 m asl). These boulders may have been deposited as the ice volume of the Deheisui glacier decreased enough that it stopped spilling into the neighboring valley and retreated, simultaneously depositing the boulders in the group B lateral moraine and the boulders in Dalijia

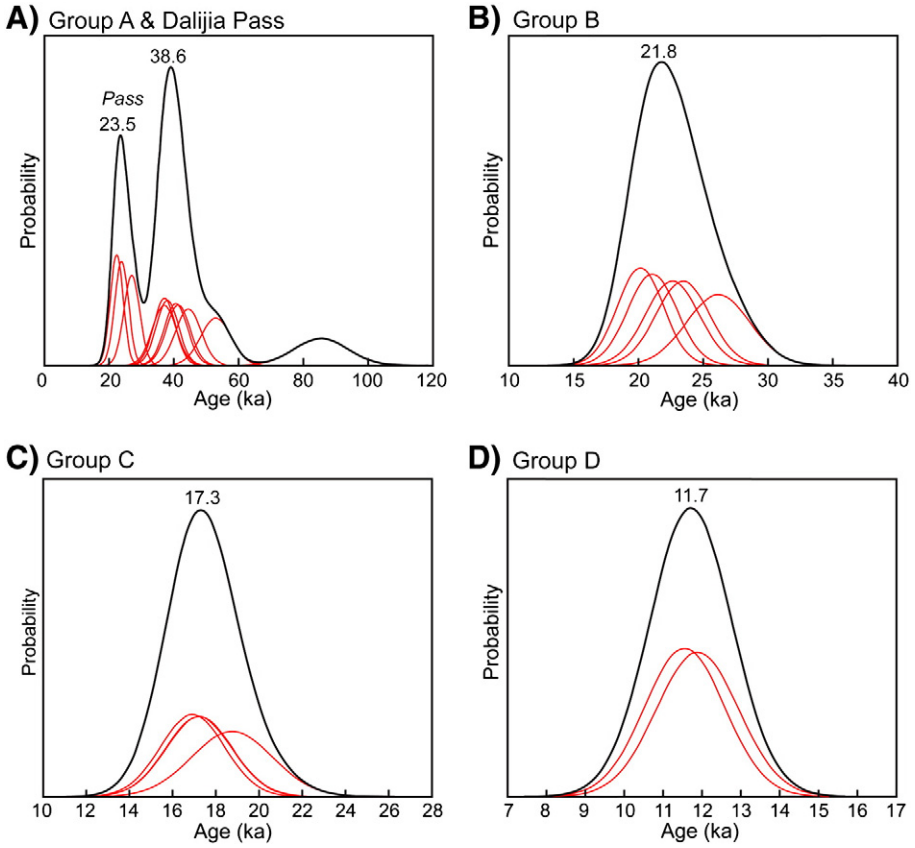


**Figure 5.** Probability plots for the different moraine groups. Red lines are Gaussian probability distributions for individual samples; the thick black lines are the sum of all individual samples. The age corresponding to the peak can be interpreted to represent the timing of a glacial event. A) Moraine group A represents a glacial event that occurred at ~38.6 ka (MIS 3). This grouping also includes the Dalijia Pass moraine which represents a similar event to group B moraines (~23.5 ka; the younger peak). B) Moraine group B represents a glacial event that occurred at ~21.8 ka (MIS 2). C) Moraine group C represents a glacial event that occurred at ~17.3 ka (MIS 2). D) Moraine group D represents a glacial event that occurred at ~11.7 ka (possibly Younger Dryas).

Pass. The only preserved terminal moraine (moraine group C) associated with the Deheisui Valley was deposited ~17.3 ka (MIS 2) and is the furthest down valley glacial landform that has been identified. A boulder located ~300 m up the valley side on the lateral moraine associated with moraine group C has a similar apparent exposure age of ~18 ka. The youngest event occurred at ~11.7 ka and is possibly associated with a stillstand in the retreat of the glacier or a limited advance. This lateral moraine is <5 km from the valley cirque.

There has been a debate about the MIS 3 glacial advance on the Tibetan Plateau. Schaefer et al. (2008) argued that the MIS 3 exposure ages could be the result of incomplete exposure in samples actually deposited earlier. However, in view of our data, it seems probable that the oldest advance recorded with the exposure data occurred during MIS 3, globally an interstadial period (Fig. 6C). During MIS 3 most of the world's glaciers were not advancing, but increased temperatures and an intensification of the summer monsoon on the Tibetan Plateau have been linked to a 40–100% increase in precipitation compared to the present (Rost, 2000; Shi et al., 2001; Shi, 2002). The winter monsoon weakens during this time and is less extensive. The reverse occurs during glacial periods—insolation decreases and the summer monsoon shrinks in extent while the winter monsoon strengthens and expands (Shi, 2002). Glacier mass balance depends on a combination of factors including but not limited to temperature, radiation, and precipitation (Rupper et al., 2009). The complexity of the feedbacks associated with these factors makes it difficult to determine the exact influence of each, but based on glacier mass-balance models, Rupper et al. (2009) argued that temperature accounted for a greater variability in glacier changes than precipitation. Yet during interstadial periods, the enhanced monsoon intensity and/or duration can lead to an increase in precipitation and a decrease in temperature, resulting in the advancement of glaciers illustrating this complexity (Rupper et al., 2009). The $\delta^{18}O$ records in Guliya ice core from the West Kunlun Mountains show that an intense temperature fluctuation occurred during MIS 3 (Thompson et al., 1997; Yao et al., 1997) (Fig. 6B). Mid-MIS 3 was an obvious cold period; the temperature dropped 5°C lower than the present (Shi et al., 2000; Shi and Yao, 2002). The paleo-temperatures inferred from the oxygen isotope record of the RM core from the Zoigê Basin on the eastern margin of the Tibetan Plateau also indicate that the mid-MIS 3 is a cold period (Wu et al., 2000). It is likely that the cold-humid climate of mid-MIS 3 produced positive glacier mass balances, therefore allowing glaciers to advance. The MIS 3 advance in the Dalijia Shan thus represents an event that is asynchronous with Northern Hemisphere glaciation. The MIS 3 advance is not limited to the northeastern region of the Tibetan Plateau but has been dated in the western regions (Fig. 6A; e.g., Pamir Mountains and Karakoram/Ladakh Range; Owen et al., 2002b; Zech et al., 2005; Abramowski et al., 2006; Dortch et al., 2010), along the southern margin of the Plateau (e.g., Mt. Everest and Nalakanaar Himal; Finkel et al., 2003; Owen et al., 2009, 2010; Chevalier et al., 2011) and central regions (e.g., Xainza Range and Nyainqentanggula; Owen et al., 2005; Chevalier et al., 2011).

During the global LGM (MIS 2), a cold and dry climate dominated the Tibetan Plateau. The summer monsoon weakened while the winter monsoon strengthened, temperature dropped ~6–9°C lower than the present and precipitation was only 30–70% of present values (Shi, 2002). This type of climate is not favorable for the mass balance of glaciers in small mountain ranges (Rost, 2000; Shi et al., 2000). Two advances in the Dalijia occurred during this time but it is thought that both were of limited extent. Because there is only one terminal moraine preserved it is impossible to say which advance had the farthest extent, but other mountains in the northeastern region experienced a local

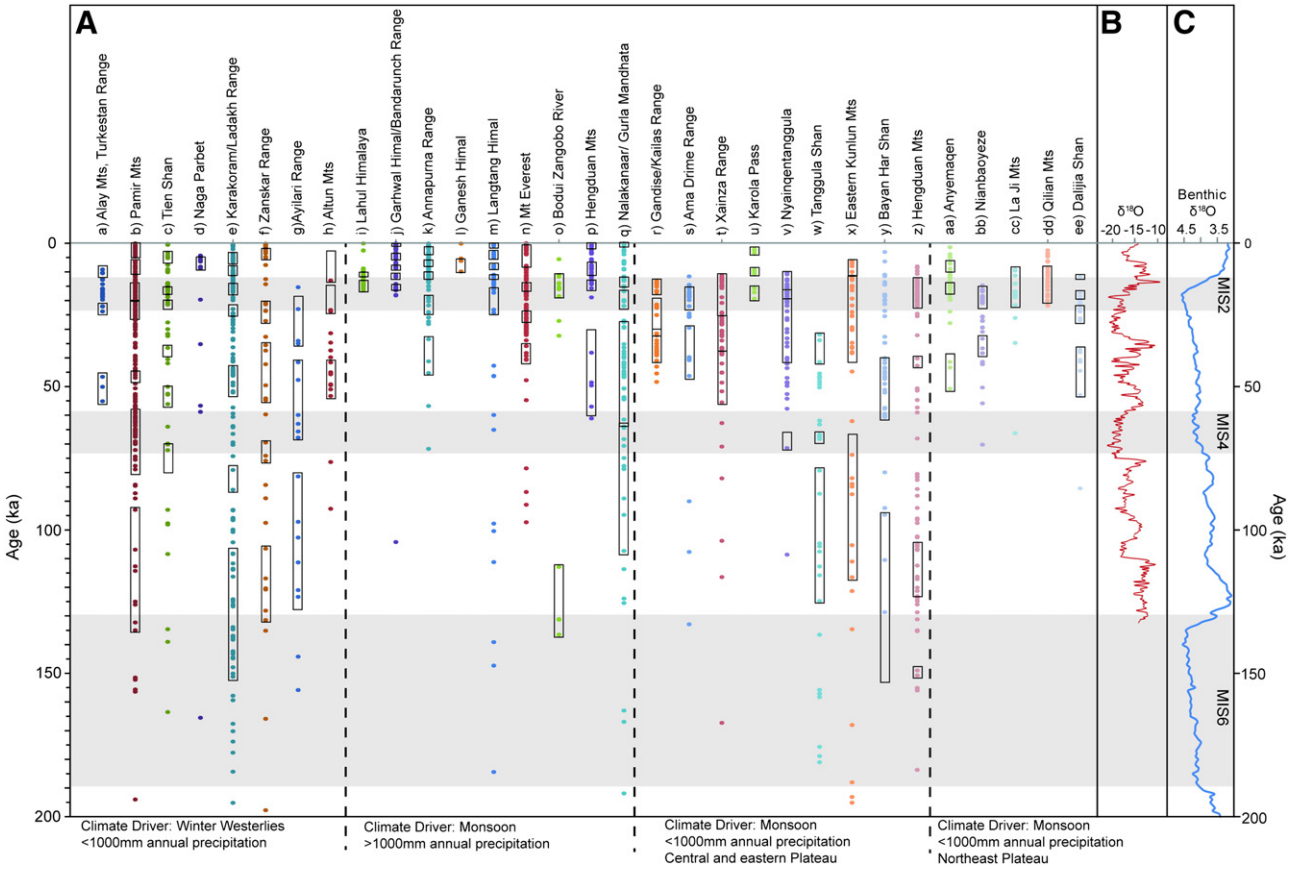


**Figure 6.** A) All published glacial boulder $^{10}$Be exposure ages (recalculated using the same scaling schemes of this paper) across the Tibetan Plateau (including ages that have been disregarded in analyses as being too young or too old). Locations of each study area can be found on Fig. 1A and the rectangles in part (A) represent the likely duration of each glacial advance based on the best estimate of the ages of moraines presented in the original publications. Data are separated based upon the climate driver, monsoon versus winter westerlies and then by location and amount of precipitation (Zhang et al., 2011). All of the data are plotted against the (B) $\delta^{18}$O record from the Guliya ice core (Thompson et al., 1997) and (C) the stacked Benthic $\delta^{18}$O curve (Lisiecki and Raymo, 2005) for the past 200 ka. Glacial periods (MIS 2, 4, 6) are highlighted by the gray boxes. Data for each location (the number in parentheses is the number of data points) are from: a) Abramowski et al. (2006) (24); b) Zech et al. (2005); Abramowski et al. (2006); Seong et al. (2009); Owen et al. (2012) (276); c) Koppes et al. (2008); Kong et al. (2009a); Li et al. (2011); Zech (2012) (65); d) Phillips et al. (2000) (14); e) Brown et al. (2002); Owen et al. (2002b, 2006a); Seong et al. (2007); Dortch et al. (2010) (173); f) Hedrick et al. (2011) (46); g) Chevalier et al. (2011) (18); h) Mériaux et al. (2004) (18); i) Owen et al. (2001) (24); j) Barnard et al. (2004a, b); Scherler et al. (2010) (54); k) Abramowski (2004); Pratt-Sitaula (2005); Zech et al. (2009) (89); l) Gayer et al. (2006) (4); m) Abramowski (2004); Barnard et al. (2006); Schaefer et al. (2008) (44); n) Aoki and Imamura (1999); Finkel et al. (2003); Owen et al. (2009); Chevalier et al. (2011) (103); o) Zhou et al. (2007) (15); p) Tschudi et al. (2003); Owen et al. (2005); Kong et al. (2009b); Strasky et al. (2009) (38); q) Owen et al. (2010); Chevalier et al. (2011) (96); r) Chevalier et al. (2011) (29); s) Chevalier et al. (2011) (21); t) Chevalier et al. (2011) (53); u) Owen et al. (2005) (11); v) Owen et al. (2005); Chevalier et al. (2011) (55); w) Schäfer et al. (2002); Owen et al. (2005); Colgan et al. (2006) (32); x) Owen et al. (2006b) (46); y) Heyman et al. (2011a) (39); z) Fu (2011); Graf et al. (2008); Schäfer (2000); Schäfer et al. (2002) (81); aa) Owen et al. (2003a) (37); bb) Owen et al. (2003a) (28); cc) Owen et al. (2003b) (15); dd) Lasserre et al. (2002), Owen et al. (2003c) (30); ee) this study (22).

LGM (>15 km from the present glacier limit) during MIS 3 and a more limited advance (<10 km from the present glacier limit) during global LGM (MIS 2; Owen et al., 2003a, b). We hypothesize that a MIS 3 terminal moraine was deposited farther downvalley but that it has since been destroyed or buried as a result of fluvial processes.

The youngest glacier event occurred during a time period when the climate was shifting towards a more humid and warmer interglacial climate lasting to the present (Li et al., 1988; Rost, 2000). This period was interrupted by abrupt brief climate excursions to a glacial climate, including the Younger Dryas (~11.5–12.8 ka; Alley et al., 1993). Younger Dryas-associated loess/paleosol sequences have been identified in the Loess Plateau directly east of the Dalijia Shan (An et al., 1993). Furthermore, Younger Dryas moraines have been identified in the eastern Tibetan Plateau (Tschudi et al., 2003); although Strasky et al. (2009) argued that periglacial surface adjustments during the Younger Dryas overprinted the glacial morphology, leading to deceptively young exposure ages of certain erratic boulders. Therefore, we suggest that the glacial event recorded in the Dalijia Shan probably corresponds to a Younger Dryas event on the Tibetan Plateau. If this event is a glacial advance rather than a stillstand, it was of even more limited extent, <4 km from the present-day cirque, than older events.

*Regional comparison*

Glacier advances appear to have varied even within the northeast Tibetan Plateau. Apparent exposure ages using $^{10}$Be have been published from the eastern Qilian Shan and La Ji Shan to the north-northwest of the Dalijia Shan, and the Anyemaqen and Nianbaoyeze Shan to the southwest of the Dalijia Shan (Lasserre et al., 2002; Owen et al., 2003a,b,c). These mountain ranges have a similar climate, with mean annual precipitation varying from 200 mm/yr in the La Ji Shan to 1000 mm/yr in the Nianboyeze. Most (~80%) of the precipitation falls during the summer. Average elevation ranges from ~5200 m in the eastern Qilian Shan to ~6200 m in the Anyemaqen. The eastern Qilian Shan and Anyemaqen are the only two ranges that are high enough to foster glacier development in the current climate regime (Lasserre et al., 2002; Owen et al., 2003a,b,c).

Numerical dating of glacial landforms provides no evidence for glaciations older than MIS 3 in any of the mountain ranges in the northeastern Tibetan Plateau (Fig. 7). Prior to the use of cosmogenic nuclide exposure-age dating, researchers thought that oldest glaciations were of MIS 14 age in the Dalijia Shan (relative age based on correlation) (Li and Pan, 1989), Last Glacial in the Anyemaqen Shan (relative age)

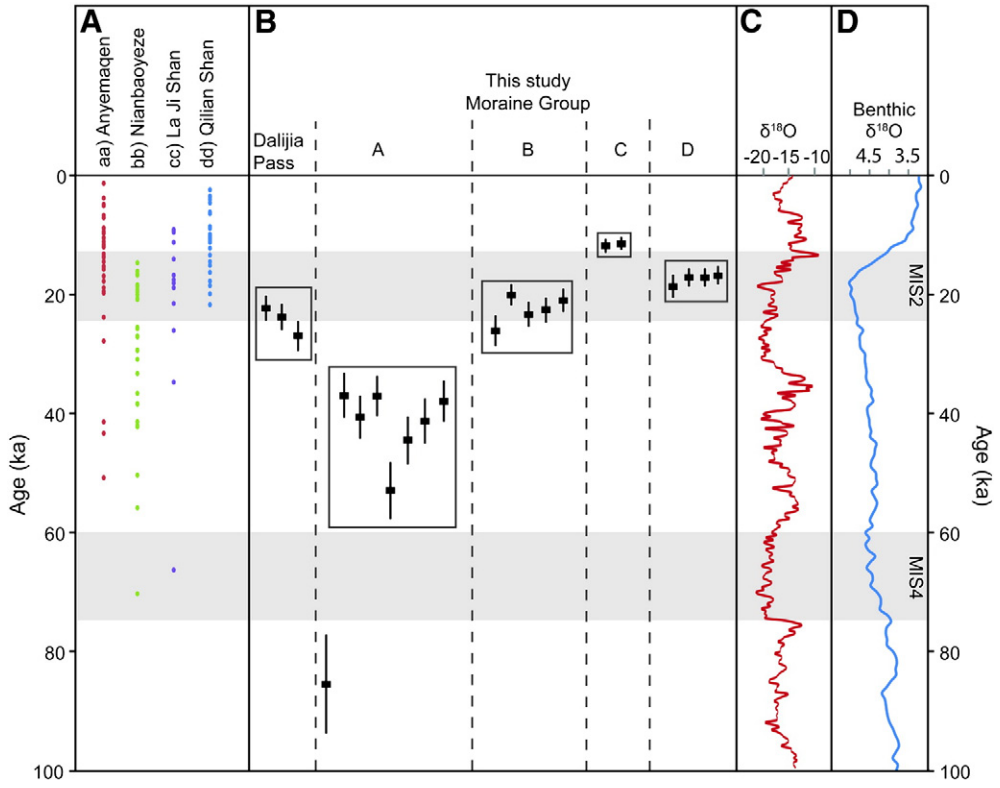


**Figure 7.** Comparison of $^{10}$Be exposure ages (with error bars) in the Dalijia Shan (B) with published exposure ages from (A) nearby mountain ranges in the NE Tibetan Plateau. The locations of each study area can be found in Fig. 1A. All of the data are plotted against the (C) $\delta^{18}$O record from the Guliya ice core (Thompson et al., 1997) and (D) the stacked Benthic $\delta^{18}$O curve (Lisiecki and Raymo, 2005) for the past 100 ka. Glacial periods are highlighted by the gray boxes (MIS 2 and MIS 4).

(Wang, 1987), older than 200 ka in the Nianboyeze (relative age based on correlation) (Lehmkuhl and Liu, 1994), and MIS 12 (ESR age) in the eastern Qilian Shan (Zhou et al., 2002). The absence of older glaciations is either due to the fact that they did not occur or that they were not preserved during later periods of heavier precipitation and/or more extensive glacial advances. The Nianbaoyeze, Anyemaqen, and Dalijia Shan share similar glaciation histories, each with advances occurring in both MIS 3 and MIS 2. The Anyemaqen also records a third advance during the early Holocene (~9 ka)—this is also the highest range of those discussed here. The La Ji and eastern Qilian Shan do not have any glaciations older than MIS 2. All of these mountain ranges are impacted by the same climate systems albeit the mean annual precipitation varies with the average elevation, which may explain the differences in timing of glacier advances.

As with many regions across the Tibetan Plateau, the local LGM in the northeastern region was asynchronous with the global LGM. In the Anyemaqen and Nianbaoyeze Shan the MIS 3 maximum extent was ~15 km beyond the present ice extent. This is much larger than the MIS 2 advance, less than 10 km from the present glacier. It is hypothesized that the MIS 3 maximum extent in the Dalijia Shan was also the local LGM. The only terminal moraine preserved in the Deheisui Valley is the one deposited during MIS 2. It is thought that the MIS 3 terminal moraine reached farther down the valley but has since been destroyed through fluvial and/or glacial processes. Even though the La Ji Shan and eastern Qilian Shan experienced a limited MIS 2 advance, <10 km from the present day glacier, no MIS 3 terminal moraines were identified and dated in these regions. As discussed earlier, maximum glacier extent during MIS 3 is unexpected on a global scale because it is occurring during an interstadial period. The decrease in temperature during mid-MIS 3 also corresponded with an increase in precipitation which fell as snow in higher elevations, allowing the glaciers to advance. Based upon variations in the $\delta^{18}$O record, Shi et al. (2001) estimated that precipitation in MIS 3 was 40 to >100% higher than the present.

Even though the exact timing of events was not the same, the mountain ranges in the northeastern Tibetan Plateau appear to have a broadly similar glacial history. The glacial history of this region on the northern boundary of the summer monsoon influence can be compared to the rest of the Tibetan Plateau in order to gain a better idea of the synchroneity of glaciations across the Plateau and the factors that contribute to any asynchroneity.

## Conclusion

In order to determine the timing of glacial events in the Dalijia Shan along the northeastern margin of the Tibetan Plateau, we analyzed 22 $^{10}$Be apparent ages from 5 moraine groups. From these data we are able to arrive at the following conclusions:

- Four glacial events are recorded in the Deheisui Valley at $37.07 \pm 3.70$ to $52.96 \pm 4.70$ ka, $20.17 \pm 1.79$ to $26.99 \pm 2.47$ ka, $16.92 \pm 1.49$ to $18.76 \pm 1.88$ ka, and $11.56 \pm 1.03$ to $11.89 \pm 1.06$ ka. Ice completely filled the valley at ~39 ka and probably spilled into the neighboring valley to the east. As the glacier retreated, boulders were deposited in Dalijia Pass (~23.5 ka) that are equivalent to the age of the next youngest lateral moraine (~21.8 ka). A terminal moraine from this older glaciation is not preserved. We assume it reached far downvalley and has since been destroyed or covered by fluvial processes. A ~17.3 ka terminal moraine is preserved just below the junction of the Deheisui Valley and Qitai Valley, recording the limited extent (<10 km) of the MIS 2 advance. The youngest event, ~11.7 ka, records either a small advance or a period of time when the glacier reached a stillstand during retreat, possibly recording a Younger Dryas event. Even though we are confident that only two

boulders provide reliable estimates of depositional age due to their close agreement, future work should include increasing the sampling size to better determine if this moraine is truly a Younger Dryas event, which has not been noted in many parts of the Tibetan Plateau.

- The timing of glacial events recorded in the Dalijia Shan is similar to those published from other mountain ranges in the northeastern Tibetan Plateau (Anyemaqen, Nianbaoyeze, La Ji, and Qilian Shan). MIS 3, MIS 2, and Holocene glacial events have been dated in these ranges. Comparing the published results, the timing of glacial events in the Dalijia Shan is most similar to those in the Anyemaqen and Nianbaoyeze Shan. Local LGM advances in the northeastern Tibetan Plateau are asynchronous with the global LGM; maximum glacial extent occurred during MIS 3, ~20 ka prior to the global LGM.
- Apparent exposure ages from the Dalijia Shan add to the growing database of exposure ages across the Tibetan Plateau. The oldest glaciation event (MIS 3) is much younger in the Dalijia Shan compared to the majority of the Tibetan Plateau where landforms related to the penultimate glaciation (MIS 6–8) are preserved. The timing of events is similar to other regions in the Tibetan Plateau where the climate is primarily driven by the monsoons with less than 1000 mm mean annual precipitation.

Supplementary data to this article can be found online at http://dx.doi.org/10.1016/j.yqres.2013.01.004.

## Acknowledgments

We thank Tom Clifton, Greg Chmiel and Susan Ma at PRIME Lab, Purdue University, for instruction and assistance in the laboratory. We also thank Lewis A. Owen, Jakob Heyman and an anonymous reviewer for their extremely positive, constructive and helpful comments. This work was supported by the National Natural Science Foundation of China (Grant Nos. 41171063 and 40801031), the National Science Fund for Distinguished Young Scholars (Grant No. 40925001) and Purdue University.

## References

Abramowski, U., 2004. The use of $^{10}$Be surface exposure dating of erratic boulders in the reconstruction of the late Pleistocene glaciation history of mountainous regions, with examples from Nepal and Central Asia. University of Bayreuth, PhD Thesis, 185.

Abramowski, U., Bergau, A., Seebach, D., Zech, R., Glaser, B., Sosin, P., Kubik, P.W., Zech, W., 2006. Pleistocene glaciations of Central Asia: results from $^{10}$Be surface exposure ages of erratic boulders from the Pamir (Tajikistan), and the Alay–Turkestan range (Kyrgyzstan). Quaternary Science Reviews 25, 1080–1096.

Alley, R.B., Meese, D.A., Shuman, C.A., Gow, A.J., Taylor, K.C., Grootes, P.M., White, J.W.C., Ram, M., Waddington, E.D., Mayewski, P.A., Zielinski, G.A., 1993. Abrupt increase in Greenland snow accumulation at the end of the Younger Dryas event. Nature 362, 527–529.

An, Z.S., Porter, A.C., Zhou, W.J., Lu, Y.C., Donahue, D.J., Head, M.J., Wu, X.H., Ren, J.Z., Zheng, H.B., 1993. Episode of strengthened summer monsoon climate of Younger Dryas age on the Loess Plateau of Central China. Quaternary Research 39, 45–54.

Aoki, T., Imamura, M., 1999. Reconstructing the glacial chronology based on the $^{10}$Be exposure age—the case study of the Khumbu Glacier, eastern Nepal Himalayas. Bulletin of the National Museum of Japanese History 81, 517–525.

Balco, G., 2011. Contributions and unrealized potential contributions of cosmogenic-nuclide exposure dating to glacier chronology, 1990–2010. Quaternary Science Reviews 30, 3–7.

Balco, G., Stone, J.O., Lifton, N.A., Dunai, T.J., 2008. A complete and easily accessible means of calculating surface exposure ages or erosion rates from $^{10}$Be and $^{26}$Al measurements. Quaternary Geochronology 3, 174–195.

Barnard, P.L., Owen, L.A., Finkel, R.C., 2004a. Style and timing of glacial and paraglacial sedimentation in a monsoon-influenced high Himalayan environment, the upper Bhagirathi Valley, Garhwal Himalaya. Sedimentary Geology 165, 199–221.

Barnard, P.L., Owen, L.A., Sharma, M.C., Finkel, R.C., 2004b. Late Quaternary (Holocene) landscape evolution of a monsoon-influenced high Himalayan valley, Gori Ganga, Nanda Devi, NE Garhwal. Geomorphology 61, 91–110.

Barnard, P.L., Owen, L.A., Finkel, R.C., Asahi, K., 2006. Landscape response to deglaciation in a high relief, monsoon-influenced alpine environment, Langtang Himal, Nepal. Quaternary Science Reviews 25, 2162–2176.

Brown, E.T., Bendick, R., Bourlès, D.L., Gaur, V., Molnar, P., Raisbeck, G.M., Yiou, F., 2002. Slip rates of the Karakorum fault, Ladakh, India, determined using cosmic ray exposure dating of debris flows and moraines. Journal of Geophysical Research 107 (B9), 2192.

Chevalier, M.-L., Hilley, G., Tapponnier, P., Van Der Woerd, J., Liu-Zheng, J., Finkel, R.C., Ryerson, F.J., Li, H.B., Liu, X.H., 2011. Constraints on the late Quaternary glaciations in Tibet from cosmogenic exposure ages of moraine surfaces. Quaternary Science Reviews 30, 528–554.

Chmeleff, J., von Blanckenburg, F., Kossert, K., Jakob, D., 2010. Determination of the $^{10}$Be half-life by multicollector ICP-MS and liquid scintillation counting. Nuclear Instruments and Methods in Physics Research B 268, 192–199.

Colgan, P.M., Munroe, J.S., Zhou, S.Z., 2006. Cosmogenic radionuclide evidence for the limited extent of last glacial maximum glaciers in the Tanggula Shan of the central Tibetan Plateau. Quaternary Research 65, 336–339.

Derbyshire, E., Shi, Y.F., Li, J.J., Zheng, B.X., Li, S.J., Wang, J.T., 1991. Quaternary glaciation of Tibet: the geological evidence. Quaternary Science Reviews 10, 485–510.

Desilets, D., Zreda, M., 2003. Spatial and temporal distribution of secondary cosmic-ray nucleon intensities and applications to in situ cosmogenic dating. Earth and Planetary Science Letters 206, 21–42.

Desilets, D., Zreda, M., Prabu, T., 2006. Extended scaling factors for in situ cosmogenic nuclides: new measurements at low latitude. Earth and Planetary Science Letters 246, 265–276.

Dortch, J.M., Owen, L.A., Caffee, M.W., 2010. Quaternary glaciation in the Nubra and Shyok valley confluence, northernmost Ladakh, India. Quaternary Research 74, 132–144.

Dunai, T.J., 2001. Influence of secular variation of the geomagnetic field on production rates of in situ produced cosmogenic nuclides. Earth and Planetary Science Letters 193, 197–212.

Fabel, D., Harbor, J., 1999. The use of in-situ produced cosmogenic radionuclides in glaciology and glacial geomorphology. Annals of Glaciology 28, 103–110.

Finkel, R.C., Owen, L.A., Barnard, P.L., Caffee, M.W., 2003. Beryllium-10 dating of Mount Everest moraines indicates a strong monsoon influence and glacial synchroneity throughout the Himalaya. Geology 31, 561–564.

Fu, P., 2011. Paleo-glaciations of the Shaluli Shan, southeastern Tibetan Plateau. Purdue University, Master's Thesis, p. 131.

Gayer, E., Lavé, J., Pik, R., France-Lanord, C., 2006. Monsoonal forcing of Holocene glacier fluctuations in Ganesh Himal (central Nepal) constrained by cosmogenic $^{3}$He exposure ages of garnets. Earth and Planetary Science Letters 252, 275–288.

Graf, A.A., Strasky, S., Zhao, Z.Z., Akçar, N., Ivy-Ochs, S., Kubik, P.W., Christl, M., Kasper, H.U., Wieler, R., Schlüchter, C., 2008. Glacier extension on the eastern Tibetan Plateau in response to MIS 2 cooling, with a contribution to $^{10}$Be and $^{21}$Ne methodology. In: Strasky, S. (Ed.), Glacial response to global climate changes: cosmogenic nuclide chronologies from high and low latitudes. ETH Zürich, PhD Thesis.

Han, T.L., 1989. The field evidences of a unified Quaternary continental glacier sheet in the Qinghai–Xizang Plateau. Geology Review 35, 468–478 (in Chinese, with English abstract).

Hedrick, K.A., Seong, Y.B., Owen, L.A., Caffee, M.W., Dietsch, C., 2011. Towards defining the transition in style and timing of Quaternary glaciation between the monsoon-influenced Greater Himalaya and the semi-arid Transhimalaya of Northern India. Quaternary International 236, 21–33.

Heyman, J., Stroeven, A.P., Caffee, M.W., Hättestrand, C., Harbor, J.M., Li, Y.K., Alexanderson, H., Zhou, L.P., Hubbard, A., 2011a. Palaeoglaciology of Bayan Har Shan, NE Tibetan Plateau: exposure ages reveal a MIS sing LGM expansion. Quaternary Science Reviews 30, 1988–2001.

Heyman, J., Stroeven, A.P., Harbor, J.M., Caffee, M.W., 2011b. Too young or too old: evaluating cosmogenic exposure dating based on an analysis of compiled boulder exposure ages. Earth and Planetary Science Letters 302, 71–80.

Kirchner, N., Greve, R., Stroeven, A.P., Heyman, J., 2011. Paleoglaciological reconstructions for the Tibetan Plateau during the last glacial cycle: evaluating numerical ice sheet simulations driven by GCM-ensembles. Quaternary Science Reviews 30, 248–267.

Kohl, C.P., Nishiizumi, K., 1992. Chemical isolation of quartz for measurement of in situ produced cosmogenic nuclides. Geochimica et Cosmochimica Acta 56, 3586–3587.

Kong, P., Fink, D., Na, C.G., Huang, F.X., 2009a. Late Quaternary glaciation of the Tianshan, central Asia, using cosmogenic $^{10}$Be surface exposure dating. Quaternary Research 72, 229–233.

Kong, P., Na, C.G., Fink, D., Zhao, X.T., Xiao, W., 2009b. Moraine dam related to late Quaternary glaciation in the Yulong Mountains, southwest China, and impacts on the Jinsha River. Quaternary Science Reviews 28, 3224–3235.

Koppes, M., Gillespie, A.R., Burke, R.M., Thompson, S.C., Stone, J., 2008. Late Quaternary glaciation in the Kyrgyz Tien Shan. Quaternary Science Reviews 27, 846–866.

Korschinek, G., Bergmaier, A., Faestermann, T., Gerstmann, U.C., Knie, K., Rugel, G., Wallner, A., Dillmann, I., Dollinger, G., von Gostomski, C.L., Kossert, K., Maiti, M., Poutivtsev, M., Remmert, A., 2010. A new value for the half-life of $^{10}$Be by heavy-ion elastic recoil detection and liquid scintillation counting. Nuclear Instruments and Methods in Physics Research B 268, 187–191.

Kuhle, M., 1998. Reconstruction of the 2.3 million km$^2$ late Pleistocene ice sheet on the Tibetan Plateau and its impact on the global climate. Quaternary International 45 (46), 71–108.

Kuhle, M., 2004. The high glacial (last ice age and LGM) ice cover in high and central Asia. In: Ehlers, J., Gibbard, P.L. (Eds.), Quaternary Glaciations Extent and Chronology, Part III: South America, Asia, Africa, Australia, Antarctica. Elsevier, Amsterdam, pp. 175–199.

Lal, D., 1991. Cosmic ray labeling of erosion surfaces: in situ nuclide production rates and erosion models. Earth and Planetary Science Letters 104, 424–439.

Lasserre, C., Gaudemer, Y., Tapponnier, P., Mériaux, A.-S., Van der Woerd, J., Yuan, D.Y., Ryerson, F.J., Finkel, R.C., Caffee, M.W., 2002. Fast late Pleistocene slip rate on the Leng Long Ling segment of the Haiyuan fault, Qinghai, China. Journal of Geophysical Research 107, 2276–2291.
Lehmkuhl, F., 1998. Extent and spatial distribution of Pleistocene glaciations in eastern Tibet. Quaternary International 45/46, 123–134.
Lehmkuhl, F., Liu, S.J., 1994. An outline of physical geography including Pleistocene glacial landforms of eastern Tibet (provinces Sichuan and Qinghai). GeoJournal 34, 7–30.
Lehmkuhl, F., Owen, L.A., 2005. Late Quaternary glaciation of Tibet and the bordering mountains: a review. Boreas 34, 87–100.
Lehmkuhl, F., Owen, L.A., Derbyshire, E., 1998. Late Quaternary glacial history of northeast Tibet. In: Owen, L.A. (Ed.), Mountain Glaciations, Quaternary Proceedings No. 6. John Wiley & Sons Ltd., Chichester, pp. 121–142.
Li, J.J., Pan, B.T., 1989. Quaternary glaciation in the Daligia Mountain on the northeast border of Qinghai–Xizang Plateau. International Field Workshop on Loess Geomorphological Processes and Hazards, May 25 to June 5, 1989: Journal of Lanzhou University, pp. 101–108.
Li, J.J., Feng, Z.D., Tang, L.Y., 1988. Late quaternary monsoon patterns on the Loess Plateau of China. Earth Surface Processes and Landforms 13, 125–135.
Li, Y.K., Liu, G.N., Kong, P., Harbor, J., Chen, Y.X., Caffee, M., 2011. Cosmogenic nuclide constraints on glacial chronology in the source area of the Urumqi River, Tian Shan, China. Journal of Quaternary Science 26, 297–304.
Lifton, N.A., Bieber, J.W., Clem, J.M., Evenson, P., Humble, J.E., Pyle, R., 2005. Addressing solar modulation and long-term uncertainties in scaling secondary cosmic rays for in situ cosmogenic nuclide applications. Earth and Planetary Science Letters 239, 140–161.
Lisiecki, L.E., Raymo, M.E., 2005. A Pliocene–Pleistocene stack of 57 globally distributed benthic $\delta^{18}O$ records. Paleoceanography 20, PA1003.
Mahaney, W.C., Rutter, N.W., 1992. Relative ages of the moraines of the Dalijia Shan, northwestern China. Catena 19, 179–191.
Mériaux, A.-S., Ryerson, F.J., Tapponnier, P., Van der Woerd, J., Finkel, R.C., Xu, X.W., Xu, Z.Q., Caffee, M.W., 2004. Rapid slip along the central Altyn Tagh Fault: morphochronologic evidence from Cherchen He and Sulamu Tagh. Journal of Geophysical Research 109, B06401.
Nishiizumi, K., Imamura, M., Caffee, M.W., Southon, J.R., Finkel, R.C., McAninch, J., 2007. Absolute calibration of $^{10}$Be AMS standards. Nuclear Instruments and Methods in Physics Research B 258, 403–413.
Oerlemans, J., 2005. Extracting a climate signal from 169 glacier records. Science 308, 675–677.
Owen, L.A., 2009. Latest Pleistocene and Holocene glacier fluctuations in the Himalaya and Tibet. Quaternary Science Reviews 28, 2150–2164.
Owen, L.A., Benn, D.I., 2005. Equilibrium-line altitude of the LGM for the Himalaya and Tibet: an assessment and evaluation of results. Quaternary International 138 (139), 55–78.
Owen, L.A., Gualtieri, L., Finkel, R.C., Caffee, M.W., Benn, D.I., Sharma, M.C., 2001. Cosmogenic radionuclide dating of glacial landforms in the Lahul Himalaya, northern India: defining the timing of late Quaternary glaciations. Journal of Quaternary Science 16, 555–563.
Owen, L.A., Finkel, R.C., Caffee, M.W., 2002a. A note on the extent of glaciation throughout the Himalaya during the global Last Glacial Maximum. Quaternary Science Reviews 21, 147–157.
Owen, L.A., FInkel, R.C., Caffee, M.W., Gualtieri, L., 2002b. Timing of multiple late Quaternary glaciations in the Hunza Valley, Karakoram Mountains, northern Pakistan: defined by cosmogenic radionuclide dating of moraines. Geological Society of America Bulletin 114, 593–604.
Owen, L.A., Finkel, R.C., Ma, H.Z., Spencer, J.Q., Derbyshire, E., Barnard, P., Caffee, M.W., 2003a. Timing and style of Late Quaternary glaciation in northeastern Tibet. Geological Society of America Bulletin 115, 1356–1364.
Owen, L.A., Ma, H.Z., Derbyshire, E., Spencer, J.Q., Barnard, P.L., Nian, Z.Y., Finkel, R.C., Caffee, M.W., 2003b. The timing and style of Late Quaternary glaciation in the La Ji Mountains, NE Tibet: evidence for restricted glaciation during the latter part of the Last Glacial. Zeitschrift fur Geomorphologie 47, 263–276.
Owen, L.A., Spencer, J.Q., Ma, H.Z., Barnard, P., Derbyshire, E., Finkel, R.C., Caffee, M.W., Nian, Z.Y., 2003c. Timing of Late Quaternary glaciation along the southwestern slopes of the Qilian Shan, Tibet. Boreas 32, 281–291.
Owen, L.A., Finkel, R.C., Barnard, P.L., Ma, H.Z., Katsuhiko, A., Caffee, M.W., Derbyshire, E., 2005. Climatic and topographic controls on the style and timing of Late Quaternary glaciation throughout Tibet and the Himalaya defined by $^{10}$Be cosmogenic radionuclide surface exposure dating. Quaternary Science Reviews 24, 1391–1411.
Owen, L.A., Caffee, M.W., Bovard, K.R., Finkel, R.C., Sharma, M.C., 2006a. Terrestrial cosmogenic nuclide surface exposure dating of the oldest glacial successions in the Himalayan orogen: Ladakh Range, northern India. Geological Society of America Bulletin 118, 383–392.
Owen, L.A., Finkel, R.C., Ma, H.Z., Barnard, P.L., 2006b. Late Quaternary landscape evolution in the Kunlun Mountains and Qaidam basin, northern Tibet: a framework for examining the links between glaciation, lake level changes and alluvial fan formation. Quaternary International 154–155, 73–86.
Owen, L.A., Caffee, M.W., Finkel, R.C., Seong, Y.B., 2008. Quaternary glaciation of the Himalayan–Tibetan orogeny. Journal of Quaternary Science 23, 513–531.
Owen, L.A., Robinson, R., Benn, D.I., Finkel, R.C., Davis, N.D., Yi, C.L., Putkonen, J., Li, D.W., Murray, A.S., 2009. Quaternary glaciation of Mount Everest. Quaternary Science Reviews 28, 1412–1433.
Owen, L.A., Yi, C.L., Finkel, R.C., Davis, N.K., 2010. Quaternary glaciation of Gurla Mandhata (Naimon'anyi). Quaternary Science Reviews 29, 1817–1830.
Owen, L.A., Chen, J., Hedrick, K.A., Caffee, M.W., Robinson, A.C., Schoenbohm, L.M., Yuan, Z., Li, W., Imrecke, D.B., Liu, J., 2012. Quaternary glaciation of the Tashkurgan Valley, Southeast Pamir. Quaternary Science Reviews 47, 56–72.
Pan, B.T., 1993. Quaternary glaciations on the Dalijia Shan. In: Chen, F.H., Zhang, W.X. (Eds.), Loess Stratigraphy and Quaternary Glaciations in the Gansu and Qinghai Provinces. Science Press, Beijing, pp. 96–103 (in Chinese).
Phillips, W.M., Sloan, V.F., Shroder Jr., J.F., Sharma, P., Clarke, M.L., Rendell, H.M., 2000. Asynchronous glaciation at Nanga Parbat, northwestern Himalaya Mountains, Pakistan. Geology 28, 431–434.
Porter, S., Swanson, T., 2008. $^{36}$Cl dating of the classic Pleistocene glacial record in the northeastern Cascade Range, Washington. American Journal of Science 308, 130–166.
Pratt-Sitaula, B., 2005. Glaciers, climate, and topography in the Nepalese Himalaya. University of California, Santa Barbara, PhD Thesis, p. 153.
Richards, B.W.M., 2000. Luminescence dating of Quaternary sediments in the Himalaya and high Asia: a practical guide to its use and limitations for constraining the timing of glaciation. Quaternary International 65 (66), 49–61.
Rost, K.T., 2000. Pleistocene paleoenvironmental changes in the high mountain ranges of central China and adjacent regions. Quaternary International 65 (66), 147–160.
Rupper, S., Roe, G., Gillespie, A., 2009. Spatial patterns of Holocene glacier advance and retreat in Central Asia. Quaternary Research 72, 337–346.
Schaefer, J.M., Oberholzer, P., Zhao, Z.Z., Ivy-Ochs, S., Wieler, R., Baur, H., Kubik, P.W., Schlüchter, C., 2008. Cosmogenic beryllium-10 and neon-21 dating of late Pleistocene glaciations in Nyalam, monsoonal Himalayas. Quaternary Science Reviews 27, 295–311.
Schäfer, J.M., 2000. Reconstruction of landscape evolution and continental paleoglaciations using in-situ cosmogenic nuclides: examples from Antarctica and the Tibetan Plateau. ETH Zürich, PhD Thesis.
Schäfer, J.M., Tschudi, S., Zhao, Z.Z., Wu, X.H., Ivy-Ochs, S., Wieler, R., Baur, H., Kubik, P.W., Schlüchter, C., 2002. The limited influence of glaciations in Tibet on global climate over the past 170000 yr. Earth and Planetary Science Letters 194, 287–297.
Scherler, D., Bookhagen, B., Strecker, M.R., von Blanckenburg, F., Rood, D., 2010. Timing and extent of late Quaternary glaciation in the western Himalaya constrained by $^{10}$Be moraine dating in Garhwal, India. Quaternary Science Reviews 29, 815–831.
Seong, Y.B., Owen, L.A., Bishop, M.P., Bush, A., Clendon, P., Copland, L., Finkel, R., Kamp, U., Shroder, J.F., 2007. Quaternary glacial history of the central Karakoram. Quaternary Science Reviews 26, 3384–3405.
Seong, Y.B., Owen, L.A., Yi, C.L., Finkel, R.C., 2009. Quaternary glaciation of Muztag Ata and Kongur Shan: evidence for glacier response to rapid climate changes throughout the late glacial and Holocene in westernmost Tibet. Geological Society of America Bulletin 121, 348–365.
Shen, Y.P., Kang, J.C., Zilliacus, H., 1989. Correlation of the Ice Age and loess deposit sequence in the region of the Mount Dalijia, Gansu, China. International Field Workshop on Loess Geomorphological Processes and Hazards, May 25 to June 5, 1989: Journal of Lanzhou University, pp. 109–119.
Shi, Y.F., 2002. Characteristics of late Quaternary monsoonal glaciation on the Tibetan Plateau and in East Asia. Quaternary International 97 (98), 79–91.
Shi, Y.F., Yao, T.D., 2002. MIS 3b (54–44 ka BP) cold period and glacial advance in middle and low latitudes. Journal of Glaciology and Geocryology 21, 1–9 (in Chinese, with English abstract).
Shi, Y.F., Zheng, B.X., Li, S.J., 1992. Last glaciation and maximum glaciation in the Qinghai–Xizang (Tibet) Plateau: a controversy to M. Kuhle's ice sheet hypothesis. Chinese Geographical Science 2, 293–311.
Shi, Y.F., Huang, M., Yao, T., 2000. Glaciers and Their Environments in China—the Present, Past and Future. Science Press, Beijing, pp. 9–53 (in Chinese).
Shi, Y.F., Yu, G., Liu, X.D., Li, B.Y., Yao, T.D., 2001. Reconstruction of the 30–40 ka BP enhanced Indian monsoon climate based on geological records from the Tibetan Plateau. Palaeogeography, Palaeoclimatology, Palaeoecology 169, 69–83.
Stone, J.O., 2000. Air pressure and cosmogenic isotope production. Journal of Geophysical Research 105 (B10), 23753–23759.
Strasky, S., Graf, A.A., Zhao, Z.Z., Kubik, P.W., Baur, H., Schlüchter, C., Wieler, R., 2009. Late glacial ice advances in southeast Tibet. Journal of Asian Earth Sciences 34, 458–465.
Thompson, L.G., Yao, T., Davis, M.E., Henderson, K.A., Mosley-Thompson, E., Lin, P.-N., Beer, J., Synal, H.-A., Cole-Dai, J., Bolzan, J.F., 1997. Tropical climate instability: the Last Glacial Cycle from a Qinghai–Tibetan ice core. Science 276, 1821–1825.
Tschudi, S., Schäfer, J.M., Zhao, Z.Z., Wu, X.H., Ivy-Ochs, S., Kubik, P.W., Schlüchter, C., 2003. Glacial advances in Tibet during the Younger Dryas? Evidence from cosmogenic $^{10}$Be, $^{26}$Al, and $^{21}$Ne. Journal of Asian Earth Sciences 22, 301–306.
Wang, J.T., 1987. Climatic geomorphology of the northeastern part of the Qinghai–Xizang Plateau. In: Hovermann, J., Wang, W.Y. (Eds.), Reports on the Northeastern Part of the Qinghai–Xizang (Tibet) Plateau. Science Press, Beijing, pp. 140–175.
Wang, K.L., Jiang, H., Zhao, H.Y., 2005. Atmospheric water vapor transport from westerly and monsoon over the Northwest China. Advances in Water Sciences 16, 432–438 (in Chinese, with English Abstract).
Wu, J.L., Wang, S.M., Shi, Y.F., Lei, J., 2000. Temperature estimation by oxygen-stable record over the past 200 ka in Zoige Basin. Science in China, Series D 43, 577–586.
Yao, T.D., Thompson, L.G., Shi, Y.F., Qin, D.H., Jiao, K.Q., Yang, Z.H., Tian, L.D., Thompson, E.M., 1997. Climate variation since the last interglaciation recorded in the Guliya ice core. Science in China, Series D 40, 662–668.
Zech, R., 2012. A late Pleistocene glacial chronology from the Kitschi-Kurumdu Valley, Tien Shan (Kyrgyzstan), based on $^{10}$Be surface exposure dating. Quaternary Research 77, 281–288.
Zech, W., Glaser, B., Abramowski, U., Dittmar, C., Kubik, P.W., 2003. Reconstruction of the Late Quaternary Glaciation of the Macha Khola valley (Gorkha Himal, Nepal) using relative and absolute ($^{14}$C, $^{10}$Be, dendrochronology) dating techniques. Quaternary Science Reviews 22, 2253–2265.

Zech, R., Abramowski, U., Glaser, B., Sosin, P., Kubik, P.W., Zech, W., 2005. Late Quaternary glacial and climate history of the Pamir Mountains derived from cosmogenic $^{10}$Be exposure ages. Quaternary Research 64, 212–230.

Zech, R., Zech, M., Kubik, P.W., Kharki, K., Zech, W., 2009. Deglaciation and landscape history around Annapurna, Nepal, based on $^{10}$Be surface exposure dating. Quaternary Science Reviews 28, 1106–1118.

Zhang, W., Cui, Z.J., Li, Y.K., 2005. The glacial extent and glacial advance/retreat asynchronicity in East Asia during Last Glaciation. Journal of Geographical Sciences 15, 293–304.

Zhang, W., Cui, Z.J., Li, Y.C., 2006. Review of the timing and extent of glaciers during the last glacial cycle in the bordering mountains of Tibet and in East Asia. Quaternary International 154 (155), 32–43.

Zhang, J.W., Chen, F.H., Holmes, J.A., Li, H., Guo, X.Y., Wang, J.L., Li, S., Lü, Y.B., Zhao, Y., Qiang, M.R., 2011. Holocene monsoon climate documented by oxygen and carbon isotopes from lake sediments and peat bogs in China: a review and synthesis. Quaternary Science Reviews 30, 1973–1987.

Zheng, B.X., Rutter, N., 1998. On the problem of Quaternary glaciations, and the extent and patterns of Pleistocene ice cover in the Qinghai–Xizang (Tibet) Plateau. Quaternary International 45 (46), 109–122.

Zheng, B.X., Xu, Q.Q., Shen, Y.P., 2002. The relationship between climate change and Quaternary glacial cycles on the Qinghai–Tibetan Plateau: review and speculation. Quaternary International 97 (98), 93–101.

Zhou, S.Z., Li, J.J., Zhang, S.Q., 2002. Quaternary glaciation of the Bailing River Valley. Qilian Shan: Quaternary International 97 (98), 103–110.

Zhou, S.Z., Li, J.J., Zhang, S.Q., Zhao, J.D., Cui, J.X., 2004. Quaternary glaciations in China. In: Ehlers, J., Gibbard, P.L. (Eds.), Quaternary Glaciations — Extent and Chronology, Part III: South America, Asia, Africa, Australia, Antarctica. Elsevier, Amsterdam, pp. 105–113.

Zhou, S.Z., Xu, L.B., Colgan, P.M., Mickelson, D.M., Wang, X.L., Wang, J., Zhong, W., 2007. Cosmogenic $^{10}$Be dating of Guxiang and Baiyu glaciations. Chinese Science Bulletin 52, 1387–1393.